



CHORUS

This is the accepted manuscript made available via CHORUS. The article has been published as:

Manipulating anomalous Hall antiferromagnets with magnetic fields

Hua Chen, Tzu-Cheng Wang, Di Xiao, Guang-Yu Guo, Qian Niu, and Allan H. MacDonald

Phys. Rev. B **101**, 104418 — Published 26 March 2020

DOI: [10.1103/PhysRevB.101.104418](https://doi.org/10.1103/PhysRevB.101.104418)

Manipulating Anomalous Hall Antiferromagnets with Magnetic Fields

Hua Chen,^{1,2} Tzu-Cheng Wang,³ Di Xiao,⁴ Guang-Yu Guo,^{3,5} Qian Niu,⁶ and Allan H. MacDonald⁶

¹*Department of Physics, Colorado State University, Fort Collins, CO 80523, USA*

²*School of Advanced Materials Discovery, Colorado State University, Fort Collins, CO 80523, USA*

³*Department of Physics and Center for Theoretical Physics,
National Taiwan University, Taipei 10617, Taiwan*

⁴*Department of Physics, Carnegie Mellon University, Pittsburgh, PA 15213, USA*

⁵*Physics Division, National Center for Theoretical Sciences, Hsinchu 30013, Taiwan*

⁶*Department of Physics, the University of Texas at Austin, Austin, TX 78712, USA*

The symmetry considerations that imply a non-zero anomalous Hall effect (AHE) in certain non-collinear antiferromagnets also imply both non-zero orbital magnetization and a net spin magnetization. We have explicitly evaluated the orbital magnetizations of several anomalous Hall effect antiferromagnets and find that they tend to dominate over spin magnetizations, especially so when spin-orbit interactions are weak. Because of the greater relative importance of orbital magnetization the coupling between magnetic order and an external magnetic field is unusual. We explain how magnetic fields can be used to manipulate magnetic configurations in these systems, pointing in particular to the important role played by the response of orbital magnetization to the Zeeman-like spin exchange fields.

I. INTRODUCTION

We have previously¹ pointed out that spin-orbit interactions induce an anomalous Hall conductivity *i.e.* an antisymmetric contribution to the conductivity tensor $\sigma_{\alpha\beta} = \partial j_{\alpha} / \partial E_{\beta}$, in some common antiferromagnets (AFMs) with non-collinear magnetic order. Because the anomalous Hall effect (AHE) is usually associated with ferromagnetism, we refer to these systems as AHE AFMs. One way to understand the finite anomalous Hall conductivity of AHE AFMs is to view it as a time-reversal-odd pseudovector $\sigma_{\alpha}^{\text{AH}} = \epsilon_{\alpha\beta\gamma} \sigma_{\beta\gamma} / 2$ that only vanishes in magnetic systems when required to do so by some lattice symmetry. This idea of spatial symmetry controlled AHE has also been extended to collinear AFMs².

Since the total magnetization is also a time-reversal-odd pseudovector, it must be nonzero in AHE AFMs. Indeed, Mn₃Ir, the prototypical AHE AFM identified in Ref.¹, has a finite magnetization^{3,4}, as do other AHE AFMs such as Mn₃Sn and Mn₃Ge⁵⁻⁸. Precisely speaking the existence of a net magnetization makes these AHE AFMs weak ferromagnets rather than ideal antiferromagnets, for which the total magnetization exactly vanishes. It is also because of the nonzero total magnetization, that the sign of the AHE can be flipped by reversing the magnetic field direction in experiments. However, the microscopic picture of magnetization in AHE AFMs is far from clear. In particular, it is expected that typical AHE AFMs should have vanishingly small total spin magnetization due to the much larger exchange coupling than the magnetic anisotropy of sublattice moments. As a result, the orbital contribution to the total magnetization⁹⁻¹⁴ is no longer negligible, and could play a key role in determining how AHE AFMs respond to external magnetic fields.

Our goal in this work is to develop a quantitative description of manipulating the order parameter direction of AHE AFMs coherently using magnetic fields coupled

to the orbital degrees of freedom of electrons, which is appropriate for those AHE AFMs with dominating orbital magnetization over the spin contribution. To this end, we first provide a general criterion, backed by first-principles calculations, for searching for such orbital-magnetization-dominant AHE AFMs. We then point out, in the framework of relativistic spin density functional theory (SDFT), that the magnetic field reorients the order parameter through an unusual orbital-spin susceptibility, for which we give a convenient formula based on linear response theory. With these preparations, we finally explain our method for investigating field-induced coherent order parameter switching in such AHE AFMs, by keeping track of energy extrema evolution in the configuration space, and illustrate the various unusual switching behaviors by applying this approach to a toy model mimicking Mn₃Ir.

II. GROUND STATE ORBITAL AND SPIN MAGNETIZATIONS

Orbital magnetization arises from circulating electron currents. In a finite system it can be unambiguously defined as the expectation value of $-\frac{1}{2}\mathbf{j} \times \mathbf{r}$.¹⁰ In an extended system this definition of orbital magnetization becomes ambiguous because the position operator is unbounded. Historically this conundrum posed both conceptual and practical challenges, but have been fully solved recently¹¹⁻¹⁴. In particular, we now know that there are two gauge-invariant contributions to the total orbital magnetization of an extended system, due to the magnetic moments of individual Bloch wave packets and to the Berry phase modification of the electron density of states in a magnetic field, respectively^{11,15}.

To verify that orbital magnetization has a larger relative importance in AHE AFMs we have calculated both orbital and spin magnetizations in Mn₃Ir, Mn₃Pt,

TABLE I. Ground state spin and orbital magnetization (in $m\mu_B$ per formula unit) for some common AHE AFMs. The partial orbital magnetizations M_{orb}^1 and M_{orb}^2 are respectively the Bloch state orbital moment and magnetic-field-dependent density-of-states contributions.

	M_{spin}	M_{orb}^1	M_{orb}^2	$M_{\text{orb}}^{\text{tot}}$
Mn ₃ Ir	26.9	-76.7	106.1	29.7
Mn ₃ Pt	11.2	-17.0	29.4	12.2
Mn ₃ Rh	2.4	-24.0	35.0	11.0
Mn ₃ Sn	0.9	40.5	-42.5	-2.0
Mn ₃ Ge	0.9	-17.5	35.2	17.7

Mn₃Rh, Mn₃Sn, and Mn₃Ge, all AHE AFMs according to previous work^{1,5-8}, listed in Table I. The orbital magnetization M_{orb} is calculated with the zero-temperature expression given in *e.g.* Ref. 14 using Wannier interpolation of results from relativistic SDFT (see the Supplemental Material¹⁶ and references¹⁷⁻²⁶ therein), which employs exchange-correlation energy functionals that retain the structure of the non-relativistic limit^{27,28}, but adds corrections from spin-orbit coupling to the Kohn-Sham single particle equations²⁹. We find that M_{orb} is at least comparable to the total spin magnetization M_{spin} in size, and that it is much larger than the latter in certain materials, *e.g.* Mn₃Rh. This is in sharp contrast to conventional metallic ferromagnets such as Fe in which orbital magnetization is more than one order of magnitude smaller than spin magnetization. We are also aware of earlier SDFT calculations showing the importance of orbital magnetization in Mn₃Sn³⁰ prior to the establishment of a gauge-invariant form of the orbital magnetization in crystalline solids.

Interestingly, comparing M_{orb} and M_{spin} across Table I, we see that heavier elements have smaller $M_{\text{orb}}/M_{\text{spin}}$ values. This trend can be understood by taking spin-orbit coupling as a weak perturbation³¹⁻³³, as we explain below. We consider first the atomic limit in which spin-orbit coupling can be approximated by $\lambda_{\text{so}}\mathbf{L}\cdot\mathbf{S}$. Here \mathbf{L} and \mathbf{S} are the orbital and spin angular momentum operators that are proportional with appropriate g -factors to the local orbital and spin magnetic moments. It follows that magnetic order, which leads to a nonzero spin density averaged over an atomic sphere surrounding each magnetic atom, results in an effective magnetic field that couples directly to the local orbital moment. We write this effective coupling as $-\mathbf{M}_{\text{orb}}\cdot\mathbf{H}$, where $\mathbf{M}_{\text{orb}} = -g_o\mu_B\mathbf{L}/\hbar$ and $\mathbf{H} = \hbar\lambda_{\text{so}}S\hat{\Omega}/g_o\mu_B$, with S and $\hat{\Omega}$ the magnitude and the direction of the local spin density, and g_o the appropriate g -factor. The orbital magnetization is then the orbital-orbital susceptibility $\overleftrightarrow{\chi}_{\text{o}}$, a rank-2 tensor that is non-zero even in the absence of spin-orbit coupling, times this effective magnetic field. It follows that the orbital magnetization is linear in spin-orbit coupling strength in the perturbative limit.

In the case of noncollinear antiferromagnets the local orbital field \mathbf{H} is usually not along the direction of the total orbital magnetization. This can be understood as a result of the anisotropy in the local $\overleftrightarrow{\chi}_{\text{o}}$ that is allowed by symmetry. For example, the structure of Mn₃Ir has a four-fold rotational symmetry around an axis (taken as \hat{z}) through a Mn atom and perpendicular to the square formed by its four nearest neighboring Ir atoms (taken as the xy plane). There are also two mirror planes perpendicular to \hat{x} and \hat{y} , respectively. These symmetry operations will eliminate all off-diagonal elements of $\overleftrightarrow{\chi}_{\text{o}}$ and make $\chi_{\text{o}}^{xx} = \chi_{\text{o}}^{yy}$, but leave the ratio between χ_{o}^{zz} and χ_{o}^{xx} unfixed. Thus even if $\hat{n}_{111}\cdot\mathbf{H} = 0$, with \mathbf{H} parallel to the local spin magnetization and exactly coplanar for the three Mn sites in a unit cell, $\hat{n}_{111}\cdot\overleftrightarrow{\chi}_{\text{o}}\cdot\mathbf{H} \neq 0$. It is also easy to see that the contributions from the other two sites in the unit cell are the same.

When the spin-canting that produces a non-zero total spin magnetization is due to site-dependent single-ion anisotropies, one can also use a similar argument as the one above to relate the total spin magnetization to the effective field due to spin-orbit coupling. In this case the total spin magnetization is induced by the effective field \mathbf{H} through a susceptibility $\overleftrightarrow{\chi}_{\text{so}}$ that connects spins and magnetic fields coupled to orbital degrees of freedom. Since $\overleftrightarrow{\chi}_{\text{so}}$ is clearly zero in the absence of spin-orbit coupling, it must be at least linear in λ_{so} , and the spin-canting must therefore be at least of 2nd order. A special role of $\overleftrightarrow{\chi}_{\text{so}}$ is in the reorientation of the noncollinear magnetic order parameters by external magnetic fields, which will be discussed in detail below. Useful formulas for $\overleftrightarrow{\chi}_{\text{so}}$ that can be applied in model or first-principles calculations are derived in Sec. IV.

The same conclusion for the spin canting can be reached by relating $\overleftrightarrow{\chi}_{\text{so}}$ to magnetocrystalline anisotropy. Following Bruno³³, we can write the spin-orbit coupling term into an anisotropy energy

$$E_{\text{so}} = -\frac{1}{2}\mathbf{H}\cdot\overleftrightarrow{\chi}_{\text{o}}\cdot\mathbf{H} = -\frac{\hbar^2\lambda_{\text{so}}^2S^2}{2\mu_B^2}\hat{\Omega}\cdot\overleftrightarrow{\chi}_{\text{o}}\cdot\hat{\Omega}. \quad (1)$$

The anisotropy energy tensor is thus at least on the order of λ_{so}^2 . For a ferromagnet with cubic symmetry the rank-2 tensor $\overleftrightarrow{\chi}_{\text{o}}$ is isotropic and one has to go to the 4th order in λ_{so} . But for Mn₃Ir the local symmetry with respect to a Mn atom is not cubic, and as discussed above $\chi_{\text{o}}^{xx} = \chi_{\text{o}}^{yy} \neq \chi_{\text{o}}^{zz}$. This means there is either an easy axis (along \hat{z}) or an easy-plane (in xy plane) anisotropy. For Mn₃Ir it is the former. Since the antiferromagnetic nearest neighbor coupling between Mn moments prefer a coplanar arrangement of the moments, which is incompatible with the local easy axes, the local Mn moments have to cant out-of-plane. The amount of canting is proportional to the ratio between the anisotropy energy and the nearest neighbor exchange coupling. Thus the spin canting has to be at least $\propto \lambda_{\text{so}}^2$. Note that this argument does not apply to spin canting due to the anisotropic exchange interaction, or the Dzyaloshinskii-Moriya interaction (DMI), which is linear in λ_{so} .^{34,35} However,

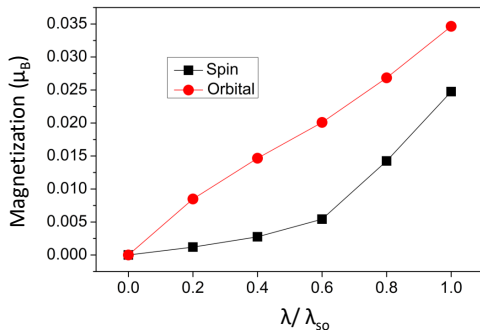


FIG. 1. Dependence of net M_{spin} and M_{orb} on spin-orbit coupling strength in Mn_3Ir . $\lambda/\lambda_{\text{so}}$ is the ratio of spin-orbit coupling strength to its realistic value.

it can be shown that in both the cubic ($X = \text{Ir}, \text{Pt}, \text{Rh}$) and the hexagonal ($X = \text{Sn}, \text{Ge}$) Mn_3X compounds DMI only plays a minor role compared to magnetocrystalline anisotropy. For the cubic compounds the DMI vectors for four nearest neighbor bonds connecting two Mn sublattices cancel each other, while for the hexagonal compounds the DMI disfavors canting³⁶ and hence only renormalizes the antiferromagnetic Heisenberg exchange coupling between Mn spins.

Although the atomic limit considerations above do not strictly apply to metallic AFMs, we expect that the general trend should still hold. As an explicit check, we calculated the total orbital and spin magnetizations of Mn_3Ir *vs.* spin-orbit coupling strength by artificially varying the speed of light when generating the fully-relativistic pseudopotentials. The results shown in Fig. 1 agree well with the qualitative picture explained above. It follows that in an AHE AFM family of given symmetries, larger $M_{\text{orb}}/M_{\text{spin}}$ values should be expected in materials with weaker, not stronger, atomic spin-orbit coupling, if the DMI is not the dominant mechanism for the spin canting.

III. MANIPULATING AFM ORDER WITH A MAGNETIC FIELD

Having established the importance of orbital magnetization in AHE AFMs, below we discuss the order parameter reorientation induced by magnetic fields within the relativistic SDFT formalism. Important differences between the present formulation and the conventional approach of solving the Landau-Lifshitz-Gilbert (LLG) equation for a classical spin model with local Zeeman coupling to external fields will be discussed at the end.

We first consider the simpler case of a ferromagnet in which the order parameter is a vector that specifies the spin-orientation $\hat{\Omega}$. Because the energy scales associated with external magnetic fields are small, it is sufficient to account only for the contribution to energy that is

of first order in \mathbf{H} , namely the coupling of \mathbf{H} to total magnetization. Minimizing total energy in the presence of a field then yields

$$0 = \delta E_{\text{ani}}(\delta\hat{\Omega}) - \delta\mathbf{M}(\delta\hat{\Omega}) \cdot \mathbf{H}, \quad (2)$$

where E_{ani} is the dependence of energy on order parameter direction in the absence of a field. When \mathbf{M} is purely due to spin its magnitude is essentially fixed at the saturation magnetization M_s . Eq. (2) then simply implies that the anisotropy field $\mathbf{H}_{\text{ani}} \equiv -\delta E_{\text{ani}}/(M_s \delta\hat{\Omega})$ cancels the external magnetic field. When \mathbf{M} is dominated by the orbital contribution, on the other hand, Eq. (2) must be generalized to

$$\mathbf{H}_{\text{ani}} + \frac{\delta\mathbf{M}_{\text{orb}}}{M_s \delta\hat{\Omega}} \cdot \mathbf{H} = 0. \quad (3)$$

To go further, we discuss the meaning of Eq. (3) within the framework of relativistic SDFT. For magnetic systems SDFT has the convenience of explicitly accounting for the Zeeman-like exchange coupling between the magnetic condensate and the Kohn-Sham quasiparticle spins in the exchange-correlation potential. Although the relativistic SDFT has some subtle disadvantages³⁷, notably a failure³⁸ to capture the interaction physics responsible for Hund's second rule, it is regularly and successfully applied and is built into common electronic structure software packages. Its practical success is likely due to the fact that the degree to which local spin alignment reduces interaction energies is not strongly altered by relativistic corrections.

In this formalism $\hat{\Omega}$ enters the exchange-correlation potential in the form of $-\Delta_{\text{ex}}\hat{\Omega} \cdot \mathbf{S} \equiv -g\mu_B \mathbf{H}_{\text{spin}} \cdot \mathbf{S}/\hbar$, where Δ_{ex} is the exchange field strength. Using a simplified notation in which the variation of Δ_{ex} within an atomic cell is left implicit, we have

$$\frac{\delta\mathbf{M}_{\text{orb}}}{M_s \delta\hat{\Omega}} = \frac{\hbar\Delta_{\text{ex}}}{g\mu_B M_s} \frac{\delta\mathbf{M}_{\text{orb}}}{\delta\mathbf{H}_{\text{spin}}} = \frac{\hbar\Delta_{\text{ex}}}{g\mu_B M_s} \overleftrightarrow{\chi}_{\text{os}}, \quad (4)$$

where $g \approx -2$ is the Lande g-factor, and $\overleftrightarrow{\chi}_{\text{os}} = \overleftrightarrow{\chi}_{\text{os}}^T$ is the *orbital-spin susceptibility* discussed further below. With this notation Eq. (2) becomes

$$\mathbf{H}_{\text{ani}} = -\frac{\hbar\Delta_{\text{ex}}}{g\mu_B M_s} \overleftrightarrow{\chi}_{\text{os}} \cdot \mathbf{H}. \quad (5)$$

It follows that when the magnetization is orbitally dominated, the anisotropy field must be balanced by an adjustment in \mathbf{M}_{orb} produced by the orbital-spin susceptibility $\overleftrightarrow{\chi}_{\text{os}}$ which, among the various magnetic susceptibility contributions identified in solid state systems³⁹⁻⁴², is the one seldom addressed in the literature^{39,43,44}. In the next section we will discuss how $\overleftrightarrow{\chi}_{\text{os}}$ can be calculated in the SDFT framework.

We now turn to the specific case of AHE AFMs, in which it is convenient to view the magnetic sublattice dependent spin-density directions $\hat{\Omega}_i$ (i labels the total N magnetic sublattices) as the order parameter. Because

the exchange coupling between local moments is strong, the relative orientations between local moments on different sublattices are normally nearly fixed. Then, as in the case of a classical rigid body, the number of parameters can be reduced to three for any N .^{45–48} The counterpart of Eq. (2) for the noncollinear case is

$$0 = \delta E_{\text{ani}}(\delta\omega) - \delta\mathbf{M}(\delta\omega) \cdot \mathbf{H}, \quad (6)$$

where ω represents the three variables parameterizing the three-dimensional rotation group $\text{SO}(3)$. For infinitesimal rotations the three components of $\delta\omega$ commute, and can be chosen as infinitesimal rotation angles around the three Cartesian axes $\delta\omega_\alpha$. It follows that

$$\begin{aligned} \frac{\delta E_{\text{ani}}}{\delta\omega_\alpha} &= \frac{\delta\mathbf{M}_{\text{orb}}}{\delta\omega_\alpha} \cdot \mathbf{H} = \mathbf{H} \cdot \sum_{i=1}^N \frac{\delta\mathbf{M}_{\text{orb}}}{\delta\hat{\Omega}_i} \cdot \frac{\delta\hat{\Omega}_i}{\delta\omega_\alpha} \quad (7) \\ &= \frac{\hbar\Delta_{\text{ex}}}{g\mu_B} H_\lambda \sum_{i=1}^N (\chi_{\text{os}}^i)_{\lambda\gamma} \epsilon_{\gamma\alpha\beta} \Omega_\beta^i. \end{aligned}$$

where Greek letters label x, y, z , $\overleftrightarrow{\chi}_{\text{os}}^i$ is the total orbital response to a local Zeeman field on sublattice i , which can be evaluated by using Eq. (9) and projecting the spin operator onto site i . The Levi-Civita symbol comes from the antisymmetric infinitesimal rotation matrix in Cartesian coordinates.

There are, however, exceptions for the applicability of Eq. (7). One example is the inverse triangular order of Mn_3Sn , which has vanishing in-plane anisotropy if one only considers the uniaxial anisotropy for each magnetic sublattice. To account for such situations it is necessary to relax the rigid body assumption. This can be done by, e.g., including a few more parameters $\{\nu_i\}$ besides the three (ω in Eq. (6)) characterizing the rigid body rotation $\hat{\Omega}$. These parameters characterize the deformation of the rigid body, and in the limit of large exchange coupling should be much smaller compared to the other three. The balance equation thus becomes

$$\begin{aligned} \frac{\delta E_{\text{ani}}}{\delta\omega_\alpha} - \frac{\delta\mathbf{M}}{\delta\omega_\alpha} \cdot \mathbf{H} &= 0, \quad (8) \\ \frac{\delta(E_{\text{ex}} + E_{\text{ani}})}{\delta\nu_i} - \frac{\delta\mathbf{M}}{\delta\nu_i} \cdot \mathbf{H} &= 0, \end{aligned}$$

which are in general hard to solve, but can sometimes be simplified with additional constraints from symmetry. One example is given in Ref. 50

$$\begin{aligned} \chi_{\text{os}}^{\alpha\beta} &= i \frac{e\hbar g\mu_B}{4} \epsilon_{\alpha\gamma\delta} \sum_{\mathbf{k}} \frac{v_{ab}^\gamma v_{ba}^\delta \sigma_{aa}^\beta}{E_{ba}} f'_a \quad (10) \\ &+ i \frac{e\hbar g\mu_B}{4} \epsilon_{\alpha\gamma\delta} \sum_{\mathbf{k}} \left[\frac{v_{aa}^\gamma (v_{ab}^\delta \sigma_{ba}^\beta - v_{ba}^\delta \sigma_{ab}^\beta) + 3\sigma_{aa}^\beta v_{ab}^\gamma v_{ba}^\delta}{E_{ab}^2} - \frac{v_{ab}^\gamma v_{bc}^\delta \sigma_{ca}^\beta + v_{ab}^\gamma \sigma_{bc}^\beta v_{ca}^\delta + \sigma_{ab}^\beta v_{bc}^\gamma v_{ca}^\delta}{E_{ab} E_{ac}} \right] f_a, \end{aligned}$$

where a, b, c are band indices, $b \neq a \neq c$ (but $b =$

With above preparations we propose the following strategy for studying coherent magnetic switching in AHE AFMs. Switching through domain nucleation and growth will be discussed elsewhere. With a microscopic Hamiltonian we can identify energy extrema that satisfy Eq. (7). These correspond to local minima, maxima, and saddle points in the $\text{SO}(3)$ parameter space. Both the positions in $\text{SO}(3)$ space and the energies of these extrema change smoothly with increasing external magnetic field. Whenever a minimum is converted to a saddle point, magnetic switching to a new minimum can proceed. For numerical implementation one can discretize the $\text{SO}(3)$ space, calculate E_{ani} , \mathbf{M}_{orb} , $\frac{\delta E_{\text{ani}}}{\delta\omega}$ and $\overleftrightarrow{\chi}_{\text{os}}^i$ at each grid point, and search for the \mathbf{H} -dependent energy extrema. To complement the tools needed for such an approach, in the next section we will give explicit formulas for the orbital-spin susceptibility, which will be used in the model example in Sec. V.

IV. CALCULATION OF ORBITAL-SPIN SUSCEPTIBILITY

The calculations described below apply a new method that we have developed to evaluate $\overleftrightarrow{\chi}_{\text{os}}$ in crystals¹⁶. To apply a uniform magnetic field to the orbital degrees of freedom we consider a periodic vector potential $\mathbf{A}(\mathbf{r}) = \frac{\mathbf{B} \times \mathbf{q}}{q^2} \sin(\mathbf{q} \cdot \mathbf{r})$, then take the $q \rightarrow 0$ limit^{14,41} with $\mathbf{q} \cdot \mathbf{B} = 0$.⁴⁹ It then follows from the linear response theory that for a grand canonical ensemble

$$\begin{aligned} \chi_{\text{os}}^{\alpha\beta} &= -\frac{e\hbar g\mu_B}{4} k_B T \epsilon_{\alpha\gamma\delta} \sum_n \quad (9) \\ &\times \text{Im} \left[\int [d\mathbf{k}] \text{tr} (G_0 v^\gamma G_0 v^\delta G_0 \sigma^\beta) \right], \end{aligned}$$

where G_0 is the Kohn-Sham thermal Green's function, \mathbf{v} is the velocity operator, σ is the spin-space Pauli matrix vector, n is a fermionic Matsubara frequency label. We note that the susceptibility is in general ensemble dependent. Conversion from the above result to that for the canonical ensemble, for example, involves evaluating the dependence of magnetization \mathbf{M} on chemical potential μ and that of μ on magnetic field \mathbf{H} .¹⁶

To convert Eq. (9) to a form more suitable for model or DFT calculations, we perform the Matsubara summation and group like terms together¹⁶.

c is allowed), and repeated indices are summed over.

$f_a = f(E_a)$ is the Fermi-Dirac distribution function, E_a is the eigenenergy for band a at a given momentum, $f'_a = \partial f(E_a)/\partial E_a$. The first term can be viewed as a correction to the g factor³⁹ and is hence separated out. But it has to be taken into account when we discuss the magnetic field induced spin-density later. Eq. (10) can be directly compared¹⁶ with the result obtained by Misra and Kleinman using a different method (Eqs. (3.40) and (3.46) in Ref. 39).

Eq. (10) is not particularly suitable for model calculations, because the energy differences in the denominators

could vanish when there are degeneracies in the occupied states. It is thus useful to rewrite Eq. (10) to a different form, in which such energy differences do not appear. The result is

$$\chi_{\text{os}}^{\alpha\beta} = i \frac{e\hbar g \mu_B}{4} (\Pi_{\text{surf}}^{\alpha\beta} + \Pi_{\text{sea},1}^{\alpha\beta} + \Pi_{\text{sea},2}^{\alpha\beta}), \quad (11)$$

where $\Pi_{\text{surf}}^{\alpha\beta}$ is a Fermi surface term, and $\Pi_{\text{sea},1}^{\alpha\beta}$, $\Pi_{\text{sea},2}^{\alpha\beta}$ are Fermi sea terms. Their expressions are

$$\begin{aligned} \Pi_{\text{surf}}^{\alpha\beta} &= -\epsilon_{\alpha\gamma\delta} \sum_{\mathbf{k}} \frac{f'_a}{E_{ab}} (v_{aa}^\gamma v_{ab}^\delta \sigma_{ba}^\beta + v_{ba}^\gamma v_{aa}^\delta \sigma_{ab}^\beta + v_{ab}^\gamma v_{ba}^\delta \sigma_{aa}^\beta), \quad a \neq b \\ \Pi_{\text{sea},1}^{\alpha\beta} &= \epsilon_{\alpha\gamma\delta} \sum_{\mathbf{k}} \frac{f_{ab}}{E_{ab}^2} (v_{aa}^\gamma v_{ab}^\delta \sigma_{ba}^\beta + v_{ba}^\gamma v_{aa}^\delta \sigma_{ab}^\beta + v_{ab}^\gamma v_{ba}^\delta \sigma_{aa}^\beta), \quad a \neq b \\ \Pi_{\text{sea},2}^{\alpha\beta} &= -\epsilon_{\alpha\gamma\delta} \sum_{\mathbf{k}} v_{ab}^\gamma v_{bc}^\delta \sigma_{ca}^\beta \left(\frac{f_a}{E_{ab}E_{ac}} + \frac{f_b}{E_{ba}E_{bc}} + \frac{f_c}{E_{ca}E_{cb}} \right), \quad a \neq b \neq c \neq a \end{aligned} \quad (12)$$

where $f_{ab} = f_a - f_b$. We now show that in the case of insulators (where Π_{surf} can be ignored at low temperatures), only cross-gap energy differences appear in the Fermi sea terms. Thus the degeneracies of filled bands will not lead to diverging integrands. First it is obvious that $\Pi_{\text{sea},1}$ only involves cross-gap energy differences E_{ab} , because of the factor f_{ab} . To see that $\Pi_{\text{sea},2}$ also has such a property we separately consider the situations of (1) $f_a = f_b = f_c$, (2) $f_a = f_b = 1$, $f_c = 0$, plus permutations of a, b, c , and (3) $f_a = f_b = 0$, $f_c = 1$, plus permutations of a, b, c . For (1) it is trivial to observe that $\frac{1}{E_{ab}E_{ac}} + \frac{1}{E_{ba}E_{bc}} + \frac{1}{E_{ca}E_{cb}} = 0$. For (2) the terms in the parentheses become $-\frac{1}{E_{ac}E_{bc}}$, which will not diverge since c is unoccupied while a and b are occupied, and other permutations of a, b, c give similar results. For (3) only the last term $\frac{1}{E_{ac}E_{bc}}$ in the parentheses is nonzero, and it will never diverge since a, b are unoccupied while c is occupied, and other permutations give similar results.

It is also interesting to make the connections between χ_{os} and the orbital magnetization more explicit. For sim-

licity we consider the insulating case at $T = 0$ so that only the Fermi sea terms in Eq. (11) are relevant. By repeatedly using the following identities

$$\begin{aligned} \langle \partial_{k_\gamma} u_{a\mathbf{k}} | u_{b\mathbf{k}} \rangle &= \frac{\hbar v_{ab}^\gamma}{E_{ab}}, \quad a \neq b \\ \langle \partial_{\Delta_\beta} u_{a\mathbf{k}} | u_{b\mathbf{k}} \rangle &= -\frac{\sigma_{ab}^\beta}{E_{ab}}, \quad a \neq b \\ \partial_{k_\gamma} H_{\mathbf{k}} &= \hbar v^\gamma, \quad \partial_{\Delta_\beta} H_{\mathbf{k}} = -\sigma^\beta, \\ \partial_{k_\gamma} E_a &= \hbar v_{aa}^\gamma, \quad \partial_{\Delta_\beta} E_a = -\sigma_{aa}^\beta, \end{aligned} \quad (13)$$

where Δ is a fictitious exchange field coupled to σ through $H_{\text{ex}} = -\Delta \cdot \sigma$, we arrive at

$$\begin{aligned} \Pi_{\text{sea},1}^{\alpha\beta} &= -\frac{\epsilon_{\alpha\gamma\delta}}{\hbar^2} \sum_{\mathbf{k}, \mathbf{a} \in \text{occu}} \partial_{\Delta_\beta} [\langle \partial_{k_\gamma} u_{a\mathbf{k}} | \partial_{k_\delta} u_{a\mathbf{k}} \rangle E_a], \quad (14) \\ \Pi_{\text{sea},2}^{\alpha\beta} &= -\frac{\epsilon_{\alpha\gamma\delta}}{\hbar^2} \sum_{\mathbf{k}, \mathbf{a} \in \text{occu}} \partial_{\Delta_\beta} [\langle \partial_{k_\gamma} u_{a\mathbf{k}} | H_{\mathbf{k}} | \partial_{k_\delta} u_{a\mathbf{k}} \rangle]. \end{aligned}$$

Therefore

$$\chi_{\text{os}}^{\alpha\beta} = \frac{g\mu_B}{2} \partial_{\Delta_\beta} \left[-\frac{ie}{2\hbar} \epsilon_{\alpha\gamma\delta} \sum_{\mathbf{k}, \mathbf{a} \in \text{occu}} \langle \partial_{k_\gamma} u_{a\mathbf{k}} | H_{\mathbf{k}} + E_a | \partial_{k_\delta} u_{a\mathbf{k}} \rangle \right] = \frac{\partial M_{\text{orb}}^\alpha}{\partial B_s^\beta}, \quad (15)$$

where $\mathbf{B}_s = 2\Delta/g\mu_B$ is an effective Zeeman field that only couples to spin degrees of freedom. Namely, the orbital-spin susceptibility can be obtained directly from taking derivative of the orbital magnetization formula

with respect to a uniform exchange field.

Before ending this section, we comment on the self-consistent-field corrections to the orbital-spin susceptibility within SDFT, when calculating the response to

a *real* Zeeman field. Note the orbital-spin susceptibility used in, e.g. Eq. (7) is not the response to actual Zeeman fields, but to order parameter re-orientation, for which we do not need to include such corrections. Taking into account the orbital response to both the Zeeman field and the associated change in the exchange field Δ defined above, we have

$$\begin{aligned}\delta\mathbf{M}_{\text{orb}} &= \overleftrightarrow{\chi}_{\text{os}} \cdot \left(\mathbf{H}_{\text{Zeeman}} + \frac{2}{g\mu_B} \delta\Delta \right), \\ \delta\Delta &= -\frac{\Delta}{M_s} \overleftrightarrow{\chi}_s \cdot \left(\mathbf{H}_{\text{Zeeman}} + \frac{2}{g\mu_B} \delta\Delta \right),\end{aligned}\quad (16)$$

where we have assumed that only the direction of the exchange field is significantly modified by the external Zeeman field. The many-body orbital-spin susceptibility within SDFT is therefore

$$\begin{aligned}\overleftrightarrow{\chi}_{\text{os}}^{\text{SDFT}} &= \\ \overleftrightarrow{\chi}_{\text{os}} \cdot \left[1 - \frac{2\Delta}{g\mu_B M_s} \left(1 + \frac{2\Delta}{g\mu_B M_s} \overleftrightarrow{\chi}_s \right)^{-1} \cdot \overleftrightarrow{\chi}_s \right].\end{aligned}\quad (17)$$

V. MODEL CALCULATIONS FOR AHE AFMS

We now give an example of the procedure proposed above using a toy model that mimics the magnetic structure of Mn_3Ir . We consider a 1/4-depleted fcc lattice (Fig. 2), with an s -orbital on each site, nearest-neighbor hopping, and sublattice-dependent exchange fields whose directions replicate the triangular antiferromagnetic order of Mn_3Ir . We add spin-orbit coupling H_{so} , being careful to respect the C_2 symmetry axis $\hat{\eta}$ along bond-dependent lines (see Fig. 2) that pass through the center of each nearest neighbor bond:

$$H_{\text{so}} = \sum_{\langle im,jn \rangle \alpha\beta} it_{\text{so}} (\hat{d}_{im,jn} \times \hat{\eta}_{mn}) \cdot \sigma_{\alpha\beta} c_{im\alpha}^\dagger c_{jn\beta} \quad (18)$$

Here ij label unit cells, mn label sublattices, $\alpha\beta$ label spin components, $\hat{d}_{im,jn}$ is a unit vector pointing from site im to site jn , and σ is the vector formed by three Pauli matrices. As discussed above the spin-orbit coupling vector $\hat{\eta}_{mn}$ is chosen to be parallel to $\mathbf{r}_{mn}^c - (\mathbf{r}_m + \mathbf{r}_n)/2$, where \mathbf{r}_{nm}^c is the mean of all neighbors of the bond mn . The band structure of this model is illustrated in Fig. 2 (b). This s - d model allows us to calculate \mathbf{M}_{orb} and $\overleftrightarrow{\chi}_{\text{os}}^i$, but not the full E_{ani} that should come from a microscopic Hamiltonian of the d electrons. We thus supplement the model with a phenomenological site-dependent uniaxial anisotropy of the exchange fields⁴ consistent with the crystal symmetry:

$$E_{\text{ani}} = -\sum_{im} \frac{K}{2} (\hat{\Omega}_{im} \cdot \hat{n}_m)^2, \quad (19)$$

where $\hat{\Omega}_{im}$ is the direction of the local exchange field on each site, and \hat{n}_m are the directions of the local easy axes on the three sublattices. $\hat{n}_{1,2,3} = \hat{x}, \hat{y}, \hat{z}$. We follow the

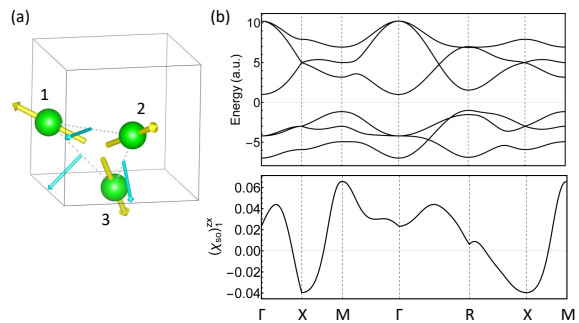


FIG. 2. (a) Structure of a s - d model resembling Mn_3Ir with its bands shown in (b). The smaller arrows in (a) represent the C_2 axes $\hat{\eta}_{mn}$ in Eq. (18).

prescription given at the end of Sec. III: We calculate E_{ani} , \mathbf{M}_{orb} , $\frac{\delta E_{\text{ani}}}{\delta \omega}$, and $\overleftrightarrow{\chi}_{\text{os}}^i$ for different configurations of the exchange field directions $\hat{\Omega}_{im}$ obtained by rotating them while fixing their relative orientations.

Consider the starting ground state configuration with \mathbf{M}_{orb} along the (111) direction, and site-dependent exchange fields with 120° relative orientations in a perpendicular plane. The eight equivalent (111) directions have identical energy minima in the absence of a magnetic field. We apply a field \mathbf{H} along the $(\bar{1}\bar{1}1)$, with the expectation that with increasing H the system will eventually switch to a configuration with a parallel \mathbf{M}_{orb} . Based on symmetry considerations we focus on the path in $\text{SO}(3)$ defined by rotation around the $(\bar{1}01)$ direction with angle θ . If the order parameter were that of an ordinary ferromagnet, E_{ani} would, in the absence of a magnetic field, have four equivalent minima along this path at $\theta = 0, \arccos(-1/3) \approx 109.47^\circ, 180^\circ$ and $\arccos(-1/3) + 180^\circ$ corresponding to four of the eight (111) directions. However, plotting our E_{ani} vs. θ in Fig. 3 (b) shows only two energy minima located at the first two rotation angles. The other two orientations differ in the chirality of the three exchange fields and do not have the same energy. Among the two remaining minima, $\theta = \arccos(-1/3)$ rotates the (111) plane normal to the $(\bar{1}\bar{1}\bar{1})$ direction. However, \mathbf{M}_{orb} is surprisingly rotated *oppositely* to the $(\bar{1}\bar{1}\bar{1})$ direction. (Similar behaviors exist in Mn_3Sn and Mn_3Ge ³⁶). Thus the magnetic switching induced by a field along $(\bar{1}\bar{1}\bar{1})$ corresponds to reaching the minimum at $\theta = \arccos(-1/3)$ through the saddle point initially at $\theta \approx 55^\circ$.

Fig. 3 (c) shows the energies of these three extrema as a function of H . As H increases, the energy of the final $\theta = \arccos(-1/3)$ state moves below that of the initial minimum, and the latter eventually disappears after merging with the saddle point. At this time the magnetization configuration will switch to the final state $\theta = \arccos(-1/3)$.

Switching between time-reversed states for non-collinear AHE AFMs is more complicated since it may

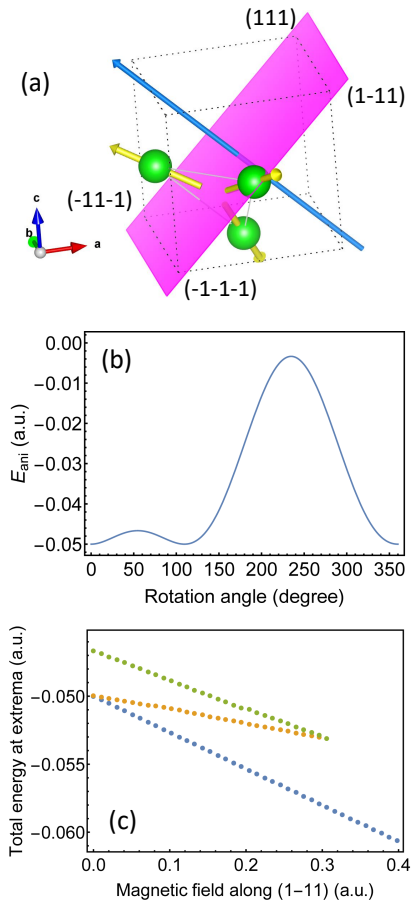


FIG. 3. (a) Rigid counterclockwise rotation of the non-collinear order parameter with respect to the $(\bar{1}01)$ direction. The unrotated structure has orbital magnetization along (111) . (b) Anisotropy energy vs. rotation angle. (c) Total energy at three lowest extrema along the rotation path vs. strength of an external magnetic field along $(1\bar{1}1)$.

not be able to be achieved through a single rotation around a fixed axis. We have already shown for the model above that such a switching cannot be achieved through a single π rotation with respect to the $(\bar{1}01)$ axis. Actually it can be realized through a single π rotation only when the rotation axis is parallel to the ground state total magnetization. This switching path has higher barriers, however, because it causes the local moments to deviate more significantly from their local easy axes. A more probable switching process consists of three segments which rotate \mathbf{M}_{orb} from (111) to $(\bar{1}\bar{1}\bar{1})$ by going through two other equivalent (111) directions, e.g., $(111) \rightarrow (1\bar{1}1) \rightarrow (1\bar{1}\bar{1}) \rightarrow (\bar{1}\bar{1}\bar{1})$. In general one needs to consider the 3 degrees of freedom of $\text{SO}(3)$, at least locally, in order to determine the smooth switching path connecting two time-reversed states. We emphasize that this nontrivial switching path can also be manifested in a static manner, through e.g. the structure of domain walls separating time-reversed states in AHE AFMs.

Moreover, in the presence of a magnetic field the idealized rotation path discussed above will smoothly deform and for sufficiently strong fields will switch directly. Figure 4 shows an example of field-induced deformation of the switching path, which plots the modulus of $\frac{\delta E}{\delta \omega}$ along the same path as in Fig. 3, but with the magnetic field along $(\bar{1}\bar{1}\bar{1})$ direction. One can see that at finite H the minimum originally at $(\bar{1}\bar{1}\bar{1})$ shifts to larger θ . Such deformation is also relevant to the structure and dynamics of magnetic domain walls driven by magnetic fields in AHE AFMs.

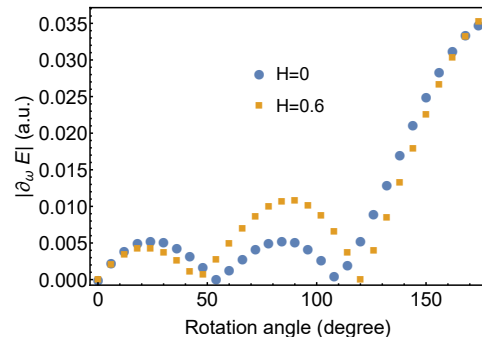


FIG. 4. Modulus of the function $\delta E/\delta \omega$ vs. the rotation angle at zero and finite magnetic fields along $(\bar{1}\bar{1}\bar{1})$.

VI. DISCUSSION

We have been ignoring spin contributions to the coupling with \mathbf{H} . Taking the spin canting into account leads to two additional effects in our theory: (1) The canting-induced spin magnetization is nonzero and can depend in a nontrivial way on the global orientation of the magnetic configuration. (2) In certain cases the magnetic anisotropy energy depends critically on the spin canting. Here we focus on the first effect since the 2nd has been discussed at the end of Sec. III.

Both the external magnetic field and spin-orbit coupling effects can lead to spin canting by competing with the exchange coupling between localized spins. When the former is much smaller than the latter, which is usually the case for canted antiferromagnets, the canting-induced spin magnetization in coherent order parameter switching is determined by minimizing the total energy while keeping the direction of the total magnetization fixed. In this case the argument of orbital magnetization dominating over the spin magnetization in the limit of small spin-orbit coupling still applies. Even if the Zeeman energy is not much smaller than the anisotropy energy, for coherent rotation to occur it only has to be comparable to the anisotropy energy, meaning the canting induced by the Zeeman field is also as small as that due to anisotropy. Therefore we can ignore the canting-induced spin magnetization throughout the switching process if the orbital

magnetization is dominant in the ground state. More generally, spin coupling to magnetic fields can be included in our formalism in a similar way as the orbital coupling, but through the spin-spin susceptibility that can also be obtained microscopically.

Our SDFT formalism for discussing field-induced switching is formally equivalent to the LLG equation in the slow dynamics limit, which becomes a torque balance equation. A major difference between our approach and the conventional LLG-based method is how the effective fields or torques are evaluated. To use the LLG equation, a usual practice is to consider a classical Heisenberg-like model, with the Heisenberg and anisotropic exchange couplings, anisotropies, and coupling to external fields, narrowed down using symmetry and fitted to experimental data. Our method does not rely on the assumption of a Heisenberg-like classical spin model, and provides the quantities appearing in the balance equation from microscopic calculations. To certain extent the role of

orbital magnetization in coherent switching discussed in this work can be represented by an effective g -tensor of each local moment in the classical spin model. The g -tensors are not only anisotropic but also have nontrivial dependence on the direction of local moments. Such an effect is not usually considered in phenomenological spin models.

ACKNOWLEDGMENTS

The work from UT Austin is supported by DOE (DE-FG03-02ER45958, Division of Materials Science and Engineering). TCW and GYG were supported by Ministry of Science and Technology of the Republic of China (MOST 104-2112-M-002-002-MY3). DX was supported by DOE BES Grant No. DE-SC0012509. The authors are grateful to Satoru Nakatsuji, Masaki Oshikawa, Yasuhiro Tada, and Junren Shi for helpful discussions.

-
- ¹ H. Chen, Q. Niu, and A. H. MacDonald, Phys. Rev. Lett. **112**, 017205 (2014).
- ² N. Sivadas, S. Okamoto, and D. Xiao, Phys. Rev. Lett. **117**, 267203 (2016).
- ³ L. Szunyogh, B. Lazarovits, L. Udvardi, J. Jackson, and U. Nowak, Phys. Rev. B **79**, 020403(R) (2009).
- ⁴ M. D. LeBlanc, M. L. Plumer, J. P. Whitehead, and B. W. Southern, Phys. Rev. B **88**, 094406 (2013).
- ⁵ J. Kübler and C. Felser, Europhys. Lett. **108**, 67001 (2014).
- ⁶ S. Nakatsuji, N. Kiyohara, and T. Higo, Nature **527**, 212-215 (2015).
- ⁷ A. K. Nayak et al., Science Adv. **2**, e1501870 (2016).
- ⁸ N. Kiyohara, T. Tomita, and S. Nakatsuji, Phys. Rev. Appl. **5**, 064009 (2016).
- ⁹ R. Shindou and N. Nagaosa, Phys. Rev. Lett. **87**, 116801 (2001).
- ¹⁰ L. L. Hirst, Rev. Mod. Phys. **69**, 607 (1997).
- ¹¹ D. Xiao, J. Shi, and Q. Niu, Phys. Rev. Lett. **95**, 137204 (2005).
- ¹² T. Thonhauser, D. Ceresoli, D. Vanderbilt, and R. Resta, Phys. Rev. Lett. **95**, 137205 (2005).
- ¹³ D. Ceresoli, T. Thonhauser, D. Vanderbilt, and R. Resta, Phys. Rev. B **74**, 024408 (2006).
- ¹⁴ J. Shi, G. Vignale, D. Xiao, and Q. Niu, Phys. Rev. Lett. **99**, 197202 (2007).
- ¹⁵ I. Souza and D. Vanderbilt, Phys. Rev. B **77**, 054438 (2008).
- ¹⁶ See Supplemental Material for additional details, which includes Refs. 17–26
- ¹⁷ W. Feng, G. Y. Guo, J. Zhou, Y. Yao, and Q. Niu, Phys. Rev. B **92**, 144426 (2015).
- ¹⁸ G. Y. Guo, and T.-C. Wang, Phys. Rev. B **96**, 224415 (2017).
- ¹⁹ J. P. Perdew, K. Burke, M. Ernzerhof, Phys. Rev. Lett. **77**, 3865 (1996).
- ²⁰ P. Giannozzi et al., J. Phys.: Condens. Matter **21**, 395502 (2009).
- ²¹ D. R. Hamann, Phys. Rev. B **88**, 085117 (2013).
- ²² X. Wang, J. R. Yates, I. Souza, and D. Vanderbilt, Phys. Rev. B **74**, 195118 (2006).
- ²³ M. G. Lopez, D. Vanderbilt, T. Thonhauser, and I. Souza, Phys. Rev. B **85**, 014435 (2012).
- ²⁴ N. Marzari, A. A. Mostofi, J. R. Yates, I. Souza, and D. Vanderbilt, Rev. Mod. Phys. **84**, 1419 (2012).
- ²⁵ A. A. Mostofi, J. R. Yates, Y.-S. Lee, I. Souza, D. Vanderbilt, and N. Marzari, Comput. Phys. Commun. **178**, 685 (2008).
- ²⁶ A. Altland and B. Simons, *Condensed Matter Field Theory*, 2nd edition, (Cambridge University Press, Cambridge, 2010).
- ²⁷ U. von Barth and L. Hedin, J. Phys. C: Solid State Phys. **5**, 1629 (1972).
- ²⁸ A. K. Rajagopal and J. Callaway, Phys. Rev. B **7**, 1912 (1973).
- ²⁹ See for example A.H. MacDonald and S.H. Vosko, J. Phys. C **12**, 2977 (1979).
- ³⁰ L. M. Sandratskii and J. Kübler, Phys. Rev. Lett. **76**, 4963 (1996).
- ³¹ J. G. Gay and R. Richter, Phys. Rev. Lett. **56**, 2728 (1986).
- ³² P. Bruno, Phys. Rev. B, **39**, 865 (1989).
- ³³ P. Bruno, *Physical origins and theoretical models of magnetic anisotropy*. Ferienkurse des Forschungszentrums Jülich, Jülich, 1993.
- ³⁴ T. Moriya, Phys. Rev. **120**, 91 (1960).
- ³⁵ I. Dzyaloshinskii, J. Phys. Chem. Solids **4**, 241 (1958).
- ³⁶ T. Nagamiya, S. Tomiyoshi, and Y. Yamaguchi, Solid State Commun. **42**, 385 (1982).
- ³⁷ A. Crépieux and P. Bruno, Phys. Rev. B **64**, 094434 (2001).
- ³⁸ I. Galanakis, Phys. Rev. B **71**, 012413 (2005).
- ³⁹ P. K. Misra and L. Kleinman, Phys. Rev. B **5**, 4581 (1972).
- ⁴⁰ Y. Gao, S. A. Yang, and Q. Niu, Phys. Rev. B **91**, 214405 (2015).
- ⁴¹ H. Fukuyama, Prog. Theor. Phys. **42**, 1284 (1969).
- ⁴² M. Ogata and H. Fukuyama, J. Phys. Soc. Jap. **84**, 124708 (2015).
- ⁴³ L. M. Roth, J. Phys. Chem. Solids **23**, 433 (1962).
- ⁴⁴ P. K. Misra and L. M. Roth, Phys. Rev. **177**, 1089 (1969).

- ⁴⁵ A. F. Andreev and V. I. Marchenko, Phys. Usp. **23**, 21 (1980).
- ⁴⁶ T. Dombre and N. Read, Phys. Rev. B **39**, 6797 (1989).
- ⁴⁷ O. Gomonay, Phys. Rev. B **91**, 144421 (2015).
- ⁴⁸ C. Ulloa and A. S. Nunez, Phys. Rev. B **93**, 134429 (2016).
- ⁴⁹ We assume \mathbf{B} to be proportional to \mathbf{H} and use them interchangeably, although it should be kept in mind that a linear proportionality is not guaranteed in magnetically ordered materials.
- ⁵⁰ Xiao Li, Allan H. MacDonald, and Hua Chen arXiv:1902.10650.